scientific reports

Check for updates

OPEN

Sparstolonin B attenuates MRSA-induced wound and peritonitis infection: in vivo, phytochemical, and computational investigation

Ahmed M. Sayed[1,2], Karim Abdelkader[3], Mahmoud Abdelnaser[4], Ramadan Yahia[5], Entesar Ali Saber[6], Ruqaiah I. Bedaiwi[7], Omnia Magdy Hendawy[8,9], Mahmoud A. Elrehany[4] & Usama Ramadan Abdelmohsen[10,11]✉

The unprecedented dissemination of antibiotic resistance announces a close post antibiotic era, thus exploring effective alternatives is urgent. Natural products are untapped alternatives that could offer effective alternatives with low costs. Sparastolonin B (SsnB) is a natural anthracene-derivative with a reported anti-inflammatory activity; however, its potential antibacterial activity is still under-explored. Here, we investigated both antibacterial and anti-inflammatory activity of SsnB in vitro, in vivo and in silico. In vitro, SsnB showed a specific antibacterial activity against Gram-positive bacteria with MIC range of 1–4 µg/ml against *S. aureus* and *E. faecalis*. Furthermore, it displayed a profound antibacterial activity against the clinical MRSA strain K15 in both wound infection, and peritonitis infection models with overall bacterial count reductions up to 1.21 and 1.23 log-units respectively. In addition, it has significantly improved wound healing and tissue repair rates compared to the un-treated group in wound infection model. SsnB has also significantly down-regulated the expression of inflammatory mediators, TLR-2, MCP-1, CXCL-1, CXCL-2, IL-6 and IL-1β, in the treated rabbits highlighting its potential anti-inflammatory activity. Finally, in silico analysis has predicted Gyr-B as a potential target for the observed SsnB antibacterial activity. To conclude, SsnB is a promising natural compound with a dual antibacterial and anti-inflammatory activities, suggesting it as a good candidate for subsequent clinical investigation.

Keywords Sparastolonin B, Staph.aureus, Toll like receptor-2, Wound healing, Docking, Gyrase-B

The rising antibiotic resistance dilemma along with the shortage in new antibiotics discovery have hampered the effective treatment of infectious diseases. Especially, methicillin-resistant *Staphylococcus aureus* (MRSA) is a challenging pathogen responsible for different hospital-acquired, community-associated and food infections. Among them, soft tissue and wound infections, carbuncles, impetigo, abscesses, are challenging and common with reported mortality up to 37,700 cases in 2019. MRSA cannot be successfully treated with any conventional antibiotic, with the exception of the recently authorized β-lactam drugs. Anti-MRSA cephalosporins and novel β-lactams are being developed. Extracellular bacterial adhesion protein, secreted by *S. aureus* during cutaneous infections, interferes with leukocyte recruitment leading to massive inflammation that retard tissue repair and healing[1]. Moreover, *S. aureus* produces extracellular vesicles that trigger the release of cytokines and promote inflammation, ultimately resulting in the formation of abscesses[2–4]. Previous investigations have indicated that

[1]Department of Pharmacognosy, Faculty of Pharmacy, Nahda University, Beni-Suef 62513, Egypt. [2]Department of Pharmacognosy, College of Pharmacy, Almaaqal University, Basrah 61014, Iraq. [3]Department of Microbiology and Immunology, Faculty of Pharmacy, Beni-Suef University, Beni-Suef 62511, Egypt. [4]Department of Biochemistry, Faculty of Pharmacy, Deraya University, New Minya 61111, Egypt. [5]Department of Microbiology and Immunology, Faculty of Pharmacy, Badr University in Assiut, Assiut 77771, Egypt. [6]Department of Medical Sciences, Deraya University, Universities Zone, New Minya 61111, Egypt. [7]Department of Medical Laboratory Technology, Faculty of Applied Medical Sciences, University of Tabuk, 71491 Tabuk, Saudi Arabia. [8]Department of Pharmacology, Faculty of Pharmacy, Jouf University, 72341 Al Jouf, Saudi Arabia. [9]Department of Clinical Pharmacology, Faculty of Medicine, Beni-Suef University, Beni-Suef 62511, Egypt. [10]Deraya Center for Scientific Research, Deraya University, New Minya 61111, Egypt. [11]Department of Pharmacognosy, Faculty of Pharmacy, Minia University, Minya 61519, Egypt. ✉email: usama.ramadan@mu.edu.eg

Toll like receptor 2 (TLR-2) and TLR4 are crucial in the pathophysiology of infection because they are the primary signal detectors that identify microbial metabolites[5,6].

Nowadays, synthetic medications are often used, and they come with side effects including drug resistance and allergic reactions. Thus, naturally-derived substances with a dual antibacterial and anti-inflammatory actions are increasingly being considered as viable options for treating resistant *S. aureus* infections and mending wounds[7].

The Chinese herb *Sparganium stoloniferum* contains a substance called sparstolonin B (SsnB). It is well known for significantly decreasing the expression of inflammatory cytokines caused by lipopolysaccharide (LPS), including interleukin-1β (IL-1β), TNF-α, and interleukin-6 (IL-6)[8]. Additionally, through a dose-dependent mechanism mediated by TLR4, SsnB can decrease nuclear factor-kappa B (NF-κB) activation, prevent the recruitment of myeloid differentiation main response gene 88 (MyD88) to TLR4 that and reduce inflammation in mice produced by lipopolysaccharide (LPS)[9]. Moreover, the administration of LPS-induced lung diseases was significantly reduced by pretreatment with SsnB[9]. On the other hand, its antibacterial activity against challenging MRSA is still under-explored, thus needs in-depth investigation.

Thus, the goal of our research is to evaluate the dual anti-inflammatory and antibacterial potential of SsnB using excision wound model infected with MRSA. Moreover, we have used a suite of computational approaches to predict the underlying mechanism of its antibacterial activity.

Materials and methods

Bacterial strains, antibiotic resistance assessment and culture conditions

A panel of ten bacterial strains (clinical and reference strains) were used throughout the study (Table 1). *S. aureus* K10 and K15 strains were recovered from their respective pus samples using Mannitol salt agar supplemented with oxacillin (final concentration of 4 µg/ml) and further confirmed as *S. aureus* using VITEK®2 system following manufacturer guidelines. Additional two methicillin sensitive *S. aureus* reference strains and previously characterized *E. faecalis* (Table 1) were also included. The sensitivity of Gram-positive bacteria to vancomycin was assessed using broth microdilution assay as described below. In addition, two previously characterized pus-isolated *A. baumannii* (MK34 and MK22) strains and three Gram-negative reference strains (*E. coli* ATCC25922, *K. pneumoniae* ATCC700603, *P. aeruginosa* PAO1, Table 1) were used in this work.

All bacterial strains were refreshed by inoculating 50 µl from their respective glycerol stocks into 4 ml of LB broth (Hi media Laboratories Pvt. Ltd., Mumbai, India) at 37°C with shaking (200 rpm) or on LB agar plates (LB broth supplemented with 2% agar).

Minimum inhibitory and bactericidal concentrations analysis

Minimum inhibitory concentration (MIC) of sparstolonin B was screened using conventional microbroth dilution assay in Muller-Hinton broth (MH) against a panel of Gram- positive and Gram-negative bacteria (Table 1). Briefly, sparstolonin B was prepared as a stock with a final concentration of 10 mg/ml (dissolved in 40% DMSO in MH broth) and dispensed in the wells of 96-well microtiter plate to cover concentration range of (2–128 µg/ml). Afterwards, the test strains (Table 1) were added individually with final density of ~ 105 CFU/ml. The plates were then incubated at 35 °C for 18–20 h and observed for turbidity. MIC was recorded as the minimum concentration showing no growth (turbidity). Parallel control was conducted using plain 40% DMSO in MH broth. Minimum bactericidal concentration was detected by spotting 10 µl of the wells showing no turbidity in the MIC analysis on MH agar plates followed by in incubation at 35 °C for 18–20 h. The MBC corresponds to the lowest concentration that showed no growth on the plates.

Strain	Source (reference)	Resistance (reference)	Sparstolonin B MIC (µg/ml)
S. aureus K10	Clinical strain recovered from pus	Methicillin-resistant, vancomycin-sensitive (MIC = 2 µg/ml; this study)	4
S. aureus K15	Clinical strain recovered from pus	Methicillin-resistant, vancomycin-sensitive (MIC = 2 µg/ml; this study)	1
S. aureus ATCC25329	Reference strain (https://www.atcc.org/products/25923)	Methicillin-sensitive reference strain for susceptibility testing (CLSI, M2-A9 [48]	2
S. aureus ATCC43300	Reference strain (https://www.atcc.org/products/43300)	Methicillin- resistant strain	4
E. faecalis	Clinical strain recovered from urine	MDR, resistant to 8 out of 11 tested antibiotic Vancomycin-resistant (MIC ≥ 16 µg/ml; this study)	4
E. coli ATCC 25922	Reference strain (https://www.atcc.org/products/25922#related-products)	Reference strain for susceptibility testing (CLSI, M2-A9 [48]	> 128
K. pneumoniae ATCC700603	Reference strain initially isolated from hospitalized patient's urine (https://www.atcc.org/products/700603)	Reference strain for susceptibility testing (CLSI, M2-A9 [48]	> 128
P. aeruginosa PAO1	Laboratory strain derived from PAO strain	Not tested	> 128
A. baumannii MK34	Clinical strain isolated from sputum	XDR, resistant to 11 tested antibiotics	> 128
A. baumannii MK22	Clinical strain recovered from pus	MDR, resistant to 10 tested antibiotics	> 128

Table 1. The list of strains used in the current study. The table illustrates the source, resistance pattern, and MIC of sparstolnin B in µg/ml against the used strains.

In vivo *study*

Animal treatment, and ethical statement

Sixty-four adult male New Zealand Dutch strain albino rabbits (obtained from the animal house of Deraya University) were kept in polypropylene cages for the experiment, and they had unrestricted access to water and a diet of herbal pellets. The animals were housed in well-ventilated animal houses with standard laboratory conditions, including a temperature of 25 ± 2°C, a relative humidity of 44–56%, and a day-night cycle of 12:12 h, seven days before the initiation of the investigation.

The study complied with the ARRIVE guidelines and internationally accepted standards for the care and use of laboratory animals, as specified in the US guidelines (NIH publication #85–23, revised 1985).

Deraya center for scientific research approved this study, stating that the animals should not be subjected to pain during any testing phase and this study was performed in accordance with the guidelines provided by the Guide for the Care and Use of Laboratory Animals (ethical license No DCSR-02024–09). The experimental protocols were approved by Deraya center for scientific research. After the study was over, the rabbits were put to death, and their bodies were burnt at the faculty of veterinary's animal ashing portion at Minia University. To mitigate the pain threshold and minimize suffering. By the end of the experiment, all rabbits were euthanatized after an intraperitoneal injection of a ketamine-xylazine mixture.

Bacterial strain and growth condition for in-vivo study

Throughout the investigation, a strain of Methicillin-resistant *Staphylococcus aureus* (MRSA) bacterium was utilized, which was acquired from Minia University Hospital (isolated from pus). The organism was cultured at 37 °C on Mueller Hinton agar (OXOID, UK). Sterile normal saline was used to create the bacterial suspension, and it was adjusted to 1 McFarland standard (equal to 3×10^8 CFU / mL. The wound region received an even application of 20 µl of MRSA suspension for the wound model. Every rabbit had four circular incisions created on its back. Each rabbit received a 0.5 mL intraperitoneal (IP) injection of MRSA suspension as part of the peritonitis model[10].

Preparation of the test samples for the bioassay, circular excision wound mode, and experimental design

There were two sets of the study, with thirty-two rabbits each: In the first, a wound model was excised, and then an MRSA strain was injected into the wound: The model of excision wounds[11] was utilized to evaluate the ability of sparstolonin B to cure wounds. Rabbit wounds were made, and the animals were rendered unconscious by intraperitoneal injections of Ketalar® (80 mg/kg), following Tramontina et al.[12]. The back hair of the rabbits was totally shaved, and the region was subsequently disinfected with povidone iodine and 70% ethyl alcohol. A 5 mm biopsy punch was used to create a circular incision in the skin around the dorsal interscapular area. Subsequently, the MRSA strain was applied into the wound.

Thirty-two rabbits were randomly assigned into 4 groups of 8 rabbits: Groups 1: normal control, group 2: untreated wound infection, Group 3: rabbits treated topically with 25 mg/wound of Sparstolonin B and Group 4: 25 mg/wound of vancomycin. Every medication was applied topically for seven days, twice a day, and the bacterial count and healing of the wounds were assessed.

The second set involved MRSA-induced peritonitis in rabbits[13]:

Thirty-two rabbits were divided into four groups of eight each at random: Group 1 involved normal control rabbits received normal saline intraperitoneal (IP); Group 2 involved untreated peritonitis-infected rabbits; Group 3 involved rabbits treated IP with sparstolonin B (25 mg/kg); Group 4 involved treating IP with vancomycin (50 mg/Kg) After MRSA infection[14]. All treatments were given intraperitoneally once a day for three days, during which the microbial count was assessed.

Before collecting samples, all the rabbits were sacrificed on day four. A 3 ml sterile saline IP injection was used to obtain a peritoneal wash. Following the peritoneum's opening, the resultant fluid which included bacteria was pipetted off for bacterial count.

Collection of tissue samples, percentage wound closure rate

On the seventh day, entire ulcers from each group had full-thickness skin biopsies collected under anesthesia. They were sectioned into two halves, one of which was kept in RNA later for a further study of gene expression and the other in 10% formalin for a histological assessment.

Until the wound healed fully, it was observed every three days (days 0, 3, 7) using a camera (Fuji, S20 Pro, Japan). After the wound area was evaluated using Image J 1.49v 4 software (National Institutes of Health, Bethesda, MD, USA), the wound closure rate was calculated as a percentage change in the original wound area using the following formula:

$$\text{Wound closure } (\%) = \frac{(Area\ of\ wound\ on\ day\ 0 - Area\ of\ wound\ on\ day\ nth)}{Area\ of\ wound\ on\ day\ 0} \times 100$$

where n represented the order of the examination day, i. e., 3rd and 7th.

Bacterial count for in-vivo study

Viable count of bacteria was performed for both the wound and peritonitis models. Samples were taken before and after treatment for the wound and peritonitis models. The wound model was treated for seven days, while the peritonitis model was treated for 3 days. 100 mg of collected wound tissue was mechanically homogenized in 1 mL of sterile saline solution for the wound model, for peritoneal model 1 mL of the peritoneal fluid was collected. Both samples were utilized for the viable count as follow; for every sample, serial dilutions were carried

out and surface pleated on Mueller Hinton agar plates. Plates were incubated for 24 h at 37 ˚C. The numbers of bacteria were expressed as CFU / mL.

Gene expression analysis

Following the manufacturer's instructions, total ribonucleic acid (RNA) was isolated from skin tissues using the TRIzol reagent (Invitrogen, USA)[15]. The quantity of extracted RNA was determined spectrophotometrically using a NanoDrop 1000 (Thermo Scientific, Waltham, MA, USA). 1 µg of total RNA was used to reverse-transcribe complementary deoxyribonucleic acid (cDNA) using oligo-dT primers and a high-capacity reverse transcription kit (Thermo Scientific, USA).

Real-time polymerase chain reaction (PCR) was used to measure transcript levels using primers unique to each sequence listed in Table 2. Following the manufacturer's instructions, DNA copies was amplified using the SYBR Green PCR Master Mix (Thermo Scientific, USA) in a step one real-time PCR thermal cycler (Thermo Fisher, USA). Once the gene expression levels were calculated relative to GAPDH as a housekeeping gene, the comparative CT technique was utilized to quantify them.

Histopathological study

Histological evaluations of collagen deposition, fibroblast predominance, and epidermal and dermal regeneration were carried out. On the seventh day, skin specimens were removed, and the tissue was treated to create paraffin blocks. To be examined under a light microscope, serial slices of around 4–5 µm thickness were cut from the paraffin blocks, mounted on glass slides, and stained with H&E and Masson trichrome.

Computational chemical–biological networking

In silico-*based target identification* The potential target characterization of retinol was accomplished through a pharmacophore-based virtual screening using the PharmMapper platform[16]. This platform assigns a score to each molecule in the Protein Data Bank (PDB) that best fits a pharmacophore model stored in a library of ligand datasets in mol2 format. When a new molecule is submitted, its fit score is calculated for each pharmacophore, and these scores are then compared to a fit score matrix to determine their relative ranking among all pharmacophore scores. This process provides a more reliable and significant fit score compared to random pharmacophore matching. The query structure was submitted to PharmMapper in PDB format, and the results were exported as an Excel sheet, ranking the identified protein targets according to their fit scores.

Docking studies The crystal structure of *S. aureus* Gyr-B (PDB ID: 5D7C) was utilized for docking studies using AutoDock Vina[17]. The binding site and docking grid-box in each protein structure were determined based on the co-crystallized ligand. The coordinates of the grid-box were set as follows: x = 2.36, y = 32.27, z = 28.33. The root mean square deviation (RMSD) threshold for ligand-to-binding site shape matching was set at 2.0 Å. Interaction energies were determined using the Charmm force field (v.1.02), with a non-bonded cutoff distance of 10.0 Å and distance-dependent dielectric. An energy grid extending 5.0 Å from the binding site was established. The compound retinol was energy minimized within the selected binding pocket, and the editing and visualization of the generated binding poses were performed using PyMOL software[18].

Molecular dynamics simulation MD simulations were conducted using NAMD 3.0.0 software[19], which applies the Charmm-36 force field. Protein systems were constructed using the QwikMD toolkit of VMD software[20], ensuring the protein structures had no missing hydrogens, setting the protonation states of the amino acid residues to pH 7.4, and removing co-crystallized water molecules. The structures were then embedded in an orthorhombic box of TIP3P water with 0.15 M Na + and Cl- ions in a 20 Å solvent buffer. The systems were energy minimized and equilibrated for 5 ns. The parameters and topologies of the ligands were calculated using the

Genes	Accession number		Primer sequence
MCP-1	NM_001082294.1	Forward	5'-GGTCTCTGCAACGCTTCTGT-3'
		Reverse	5'-CTTTGGGACACTTGGTGCTG-3'
TLR-2	NM_001082781.1	Forward	5'-TTTGAGGCGCTCAGCCAAAC-3'
		Reverse	5'-TGCCCTCTCTCAAGTGCCTG-3'
CXCL-1	NM_001082386.1	Forward	5'-ACCGAAGTCATAGCCACGCTC-3'
		Reverse	5'-CAGCCACCACCCATCAGCTTC-3'
CXCL-2	XM_002717021.3	Forward	5'-GACCGAAGTCATAGCCACGC-3'
		Reverse	5'-CAGGAACAACCCCTGCTGAGT-3'
IL-1 β	NM_001082201.1	Forward	5'- TTCGAGGCAAGAGGCACAAC-3'
		Reverse	5'- TGTTGTAGGGTTGGCAGGAG-3'
IL-6	NM_001082064.2	Forward	5'-AGAACCATCGAGAGCATCCG-3'
		Reverse	5'-CAGCCCCGAAGTGATTCTCA-3'
GAPDH	NM_001082253.1	Forward	5'- GTTTGTGATGGGCGTGAACC-3'
		Reverse	5'- GTGGAGGCAGGGATGATGTT-3'

Table 2. Primers used for qRT-PCR.

Group	Count (CFU/mL)	
	Wound model	Peritonitis model
Untreated group II	250,142	329,643
Treated group III	14,522	20,158
Treated group IV	210	2015

Table 3. Bacterial count.

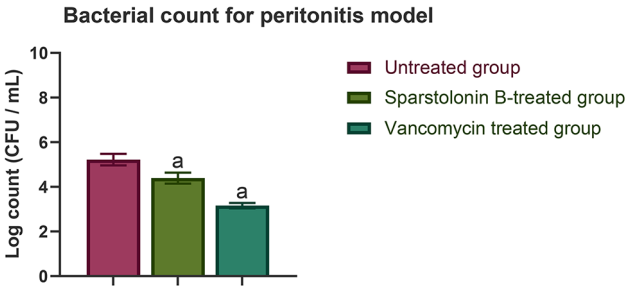

Fig. 1. Bacterial count for peritonitis model in tested groups; group 2: untreated peritonitis infection, group 3 rabbits treated IP with Sparstolonin B (25 mg/kg), and group 4 rabbits treated IP with vancomycin (50 mg/kg). A significant difference between groups is analyzed by a two-way ANOVA test. Data were expressed as mean ± SD. a $p < 0.05$ compared with the data of the untreated group.

VMD plugin Force Field Toolkit (ffTK). These generated parameters and topology files were loaded into VMD[21] to read the protein–ligand complexes accurately and conduct the simulation steps.

Binding free energy calculations The binding free energy of the docked complex was calculated using the Molecular Mechanics Poisson-Boltzmann Surface Area (MM-PBSA) method embedded in the MMPBSA.py module of AMBER18[22]. A total of 100 frames from the trajectories were processed, and the system's net energy was estimated using the following equation:

$$\Delta G \text{ Binding} = \Delta G \text{ Complex} - \Delta G \text{ Receptor} - \Delta G \text{ Inhibitor}$$

Each term in the equation involves calculating multiple energy components, including van der Waals energy, electrostatic energy, internal energy from molecular mechanics, and the polar contribution to solvation energy.

Statistical analysis

The data was displayed as mean (n = 6) ± standard deviation (SD). After doing a one-way analysis of variance (ANOVA), the Tukey-Kramar post-analysis test was performed. Graph Pad Prism 7 (Graph pad Software, San Diego, California, USA) was used for statistical calculations. In cases where $p < 0.05$ was used, the findings were regarded as significant.

Results and discussion

In-vitro minimum inhibitory and bactericidal concentrations analysis (MIC, MBC)

Sparastolonin B compound was screened for MIC and MBC against different MRSA strains by CLSI approved microbroth dilution method. The resuts revealed that, Sparastolonin B has a specific activty against Gram-positive bacteria in strain-dependant manner. For instance, Sparastolonin B displayed the maximum activity against the clinical MRSA strainK15 followed by the reference strain ATCC25329 with MIC values of 1 and 2 µg/ml repectively. MIC values was doubled against MRSA K10 **,** MRSA ATCC43300 and *E. faecalis* to be 4 µg/ml (Table 1). On the other hand, np antibacterial activity was observed against any of the tested Gram-negative bacteria. These findings suggest molecular target only found in Gram-positive bacteria.

In vivo study

Bacterial count

For the peritonitis model, untreated rabbits showed a significant increase ($p < 0.05$) in the bacterial count which was reduced dramatically ($p < 0.05$) by treatment with both Sparastolonin B and vancomycin.

Moreover, for the wound model, there was a considerable elevatation ($p > 0.05$) in the bacterial count for the untreated rabbits, whereas treatment with sparastolonin B and vancomycin revealed a marked decline ($p > 0.05$) in the bacterial count.

(Table 3) (Figs. 1 and 2).

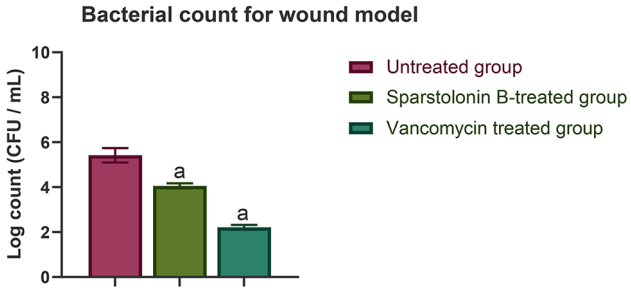

Fig. 2. Bacterial count for wound model in tested groups; group 2: untreated wound infection, group 3 rabbits treated topically with Sparstolonin B (25 mg/wound), and group 4 rabbits treated topically with vancomycin (25 mg/wound). A significant difference between groups is analyzed by a two-way ANOVA test. Data were expressed as mean ± SD. a $p < 0.05$ compared with the data of the untreated group.

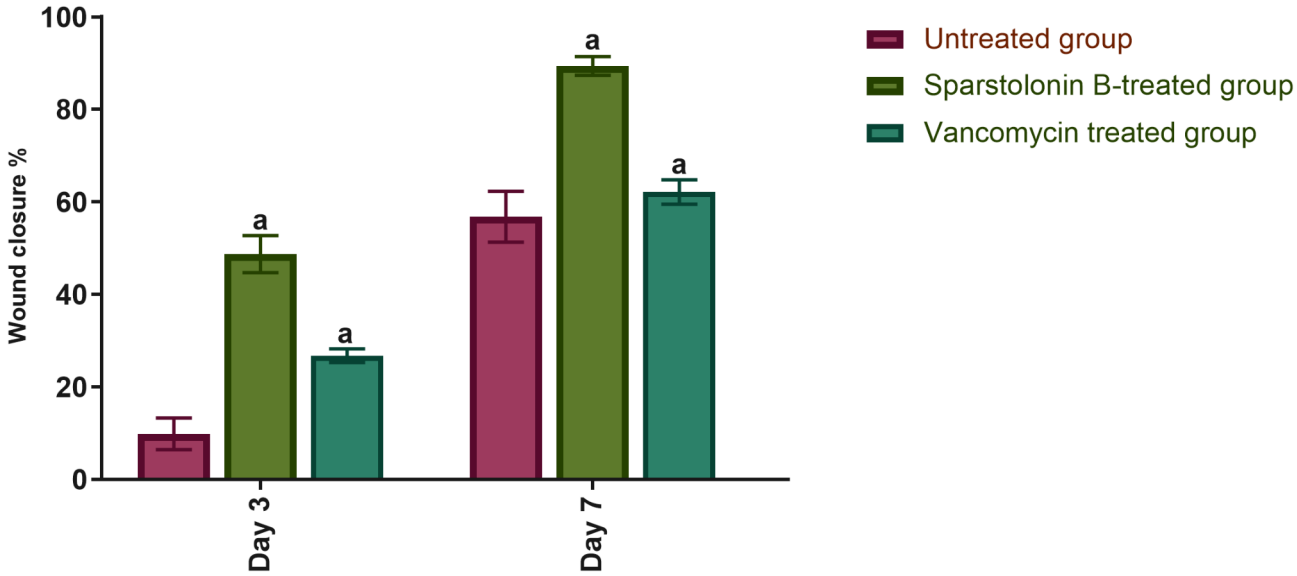

Fig. 3. Wound closure percentages in tested groups; group 2: untreated wound infection, group 3 rabbits treated topically with Sparstolonin B (25 mg/wound), and group 4 rabbits treated topically with vancomycin (25 mg/wound) over time post-injury (3 and 7 days). Significant difference between groups is analyzed by a two-way ANOVA test. Data were expressed as mean ± SD. a $p < 0.05$ compared with the data of the untreated group on the respective day.

Wound closure rate estimation

Results demonstrate that the rate of wound healing increased across all experimental groups, in a mode that depends on time. The rates of wound healing ranged from 9.8% to 56.7% in the smallest was in the untreated group and the largest in each group on day three following injury, higher in the treated ones, with significant differences between groups ($p < 0.05$). On day 7, 89% of the wounds in the group treated with sparstolonin B had closed which was substantially greater ($p < 0.05$) than the similar untreated group (Figs. 3,4).

Furthermore, on the third day following damage, the percentage of wound closure in the sparstolonin B-treated group (48%) was substantially higher ($p > 0.05$) than that in the untreated group (9%) ($p > 0.05$). Day 7 wound closure scores for the rabbits treated with sparstolonin B were 89%, vancomycin treated group (62%) with different healing percentages compared to the untreated group (56%) (Figs. 3 and 4).

Effect of sparastolonin B on gene expression of TLR-2, MCP-1, CXCL-1, CXCL-2, IL-6 and IL-1β

Figure 5 shows the mRNA expression of TLR-2 after excisional wound treatment. using Vancomycin, and Sparstolonin B. TLR-2 relative mRNA expression in skin tissues was significantly upregulated ($p > 0.05$) in untreated group in relation to normal control group.

Furthermore, there was a marked reduction ($p > 0.05$) in TLR-2 gene expression in Vancomycin ®, and Sparstolonin B treated wounds ($p > 0.05$) in comparison, to the positive control (untreated) group.

As depicted in Fig. 6, MCP-1 relative mRNA expression in skin tissues was significantly increased ($p < 0.05$) in the untreated group when compared to the normal control group. Conversely, in comparison to the positive

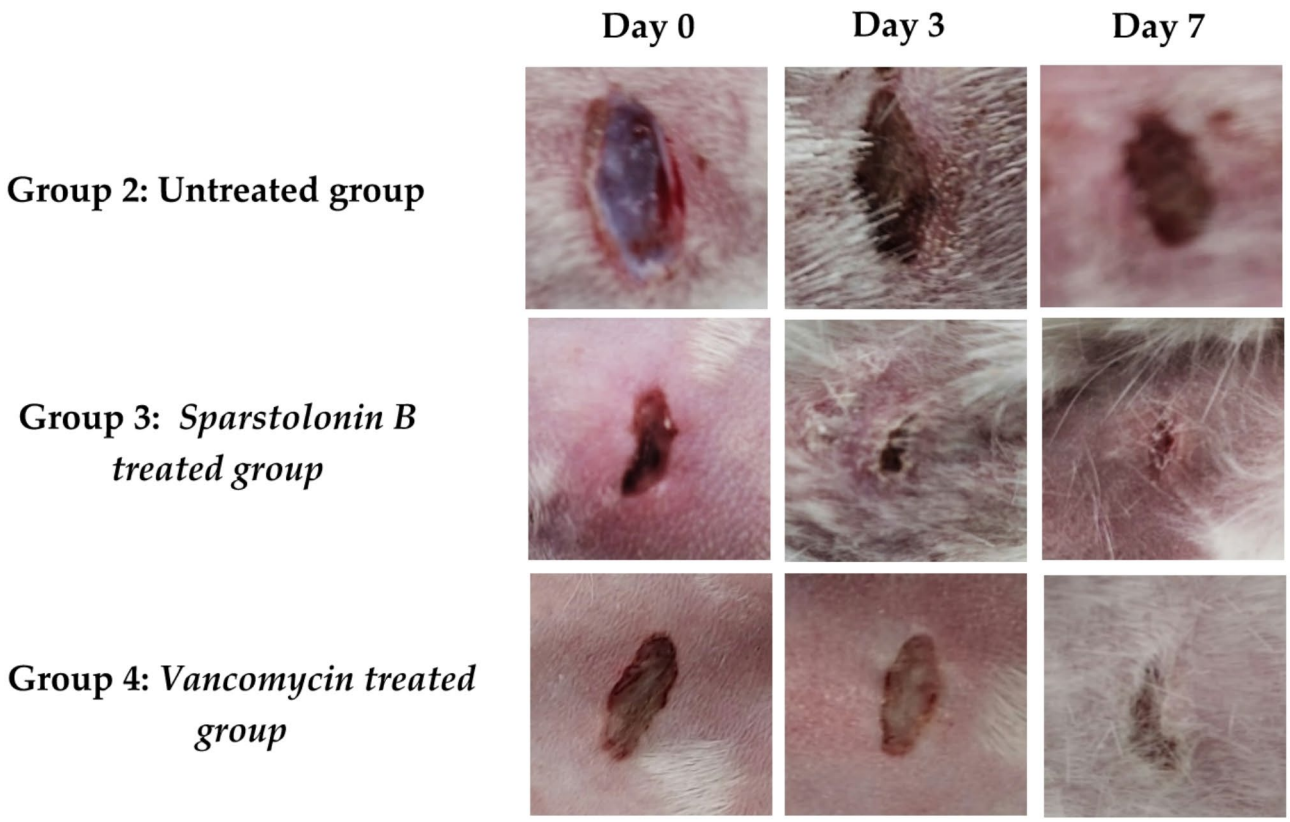

Fig. 4. Wound closure rates in tested groups; group 2: untreated wound infection, group 3 rabbits treated topically with Sparstolonin B (25 mg/wound), and group 4 rabbits treated topically with vancomycin (25 mg/wound) over time post-injury (3 and 7 days). Significant difference between groups is analyzed by a two-way ANOVA test. Data were expressed as mean ± SD. $p < 0.05$ compared with the data of the untreated group on the respective day.

control group, MCP-1 relative mRNA expression in skin tissues was significantly inhibited in wounds treated with Vancomycin, and Sparstolonin B ($p < 0.05$).

As shown in Fig. 7, the relative gene expression of CXCL-1 and CXCL-2 is Illustrated. Significant elevation in the gene expression of CXCL-1 and CXCL-2 was evident in full-thickness wounds in the untreated group when compared to the normal control group ($p < 0.05$). However, when compared to untreated wounds treatment with Vancomycin, and Sparstolonin B significantly suppressed CXCL-1 and CXCL-2 ($p < 0.05$) gene expression.

Figure 8 demonstrates the relative gene expression of proinflammatory cytokines (IL-6 and IL-1β). Compared to the normal control group, there was a significant increase in the levels of pro-inflammatory cytokines in the untreated group ($p > 0.05$). Moreover, they were inhibited significantly in groups treated with Vancomycin, and Sparstolonin B in contrast to the untreated group ($p > 0.05$).

Histopathological results

G1 (normal control)

The epidermis is the outermost layer formed of stratified squamous keratinized epithelium and the dermal connective tissue containing many hair follicles and sebaceous glands. The collagen bundles in the papillary dermis appeared as fine interlacing bundles, and in the reticular dermis appear as coarse wavy bundles arranged in different directions "Fig. 9A1,A2 ".

G 2 (untreated wound infection)

At the wound area, the epithelium is discontinuous and filled with blood clots, sloughed granulation tissue with collagen fibers compactly arranged in an abnormal pattern, extravasated RBCs and inflammatory cellular infiltration mainly neutrophils and eosinophils "Fig. 9B1,B2".

G 3 (treated with sparstolonin B extract)

Complete re-epithelization formed of many cell layers and the underlying dermal matrix had many hair follicles, and Collagen fibers appeared in a reticular pattern almost resembling that of the adjacent normal dermis. The reticular dermis contains frequent active elongated, spindle-shaped fibroblasts with basophilic cytoplasm and open-face oval nuclei "Fig. 10A1 & A2 ".

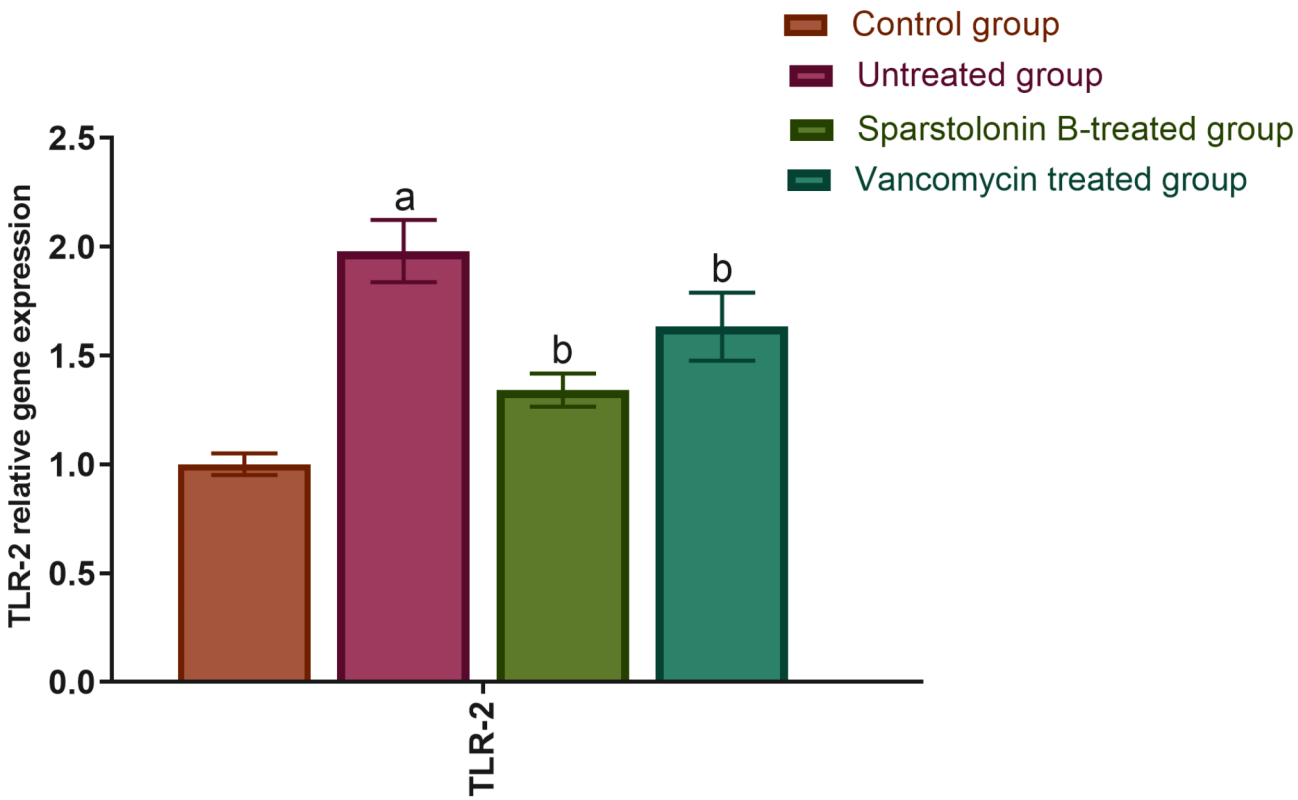

Fig. 5. Relative gene expression TLR-2 in wound tissues of various groups. After making normalization to glyceraldehyde 3-phosphate dehydrogenase (GAPDH), the data indicate a fold difference in expression relative to the natural control group and untreated group. The bars indicate the mean ± SD and are based on the results of four independent investigations. A one-way ANOVA test is employed to measure whether there is a significant change between groups, where: a,$p < 0.05$ when compared to the normal control group on a specified day, b, $p < 0.05$ when compared to the untreated group on a specified day.

G 4 (Treated with vancomycin "the standard drug in the market)

The scar tissue blocking the wound and creeping of epidermal cells trying to cover the wound, marked inflammatory cellular infiltration (mainly macrophages), and granulation tissue started to grow from the base and the wound edges to fill the gap. Disorganized dense collagen with fibers compactly arranged in an abnormal pattern resulting in distinct scarring. There were obvious active elongated, spindle-shaped fibroblasts with basophilic cytoplasm and open-face oval nuclei "Fig. 10B1,B2".

The process of healing involves three parallel, overlapping processes. steps beginning with granulation following the creation of inflammatory tissue, followed by matrix development and remodelling[23]. This approach makes use of the well-organized delicate interplay of dermal and epidermal cells regulated by keratinocytes, inflammatory cells, and chemical mediators released by fibroblasts. Capillaries multiply, mesenchymal cells proliferate, and macrophages infiltrate to produce granulation tissues, which replace the damaged dermis. Additionally, they supply the required components and sources of substrates, as well as promote and support reepithelialisation[24]. It is well known that infections in wounds have a delayed negative impact on overall outcomes, such as significant scarring, and a slower healing rate[25,26]. Open incision wounds get larger and extend due to inflammation. This conclusion is not always likely, depending on how much contractile force is present in the wound. In the current study, we used a circular biopsy punch to cut the skin of rabbits.

Moreover, it could be said that in GII the seventh days post wounding there was predominance of inflammatory phase while in GIII and GIV there was predominance of proliferative phase including decrease inflammation, reepithelization, collagen deposition and new hair follicle formation. GIII-Treated with Sparstolonin B extract " showed the best results followed by groups IV—Treated with vancomycin.

It could be said that Sparstolonin B-treated group gave the best results of accelerating wound healing through epidermal/dermal regeneration, granulation tissue thickness, and angiogenesis.

Our results expected that Sparstolonin B extract might have inflammatory ameliorative activity by controlling inflammatory mediators that are the main result of oxidative stress.

It could be concluded that rapid wound healing occurred in Sparstolonin B extract treated animals. This was in the same line of Nayeon Kim et al.[27] who reported that Sparstolonin B , was found to prevent the synthesis of inflammatory mediators and could be a candidate for promoting novel clinical substances to repair pathologic inflammation.

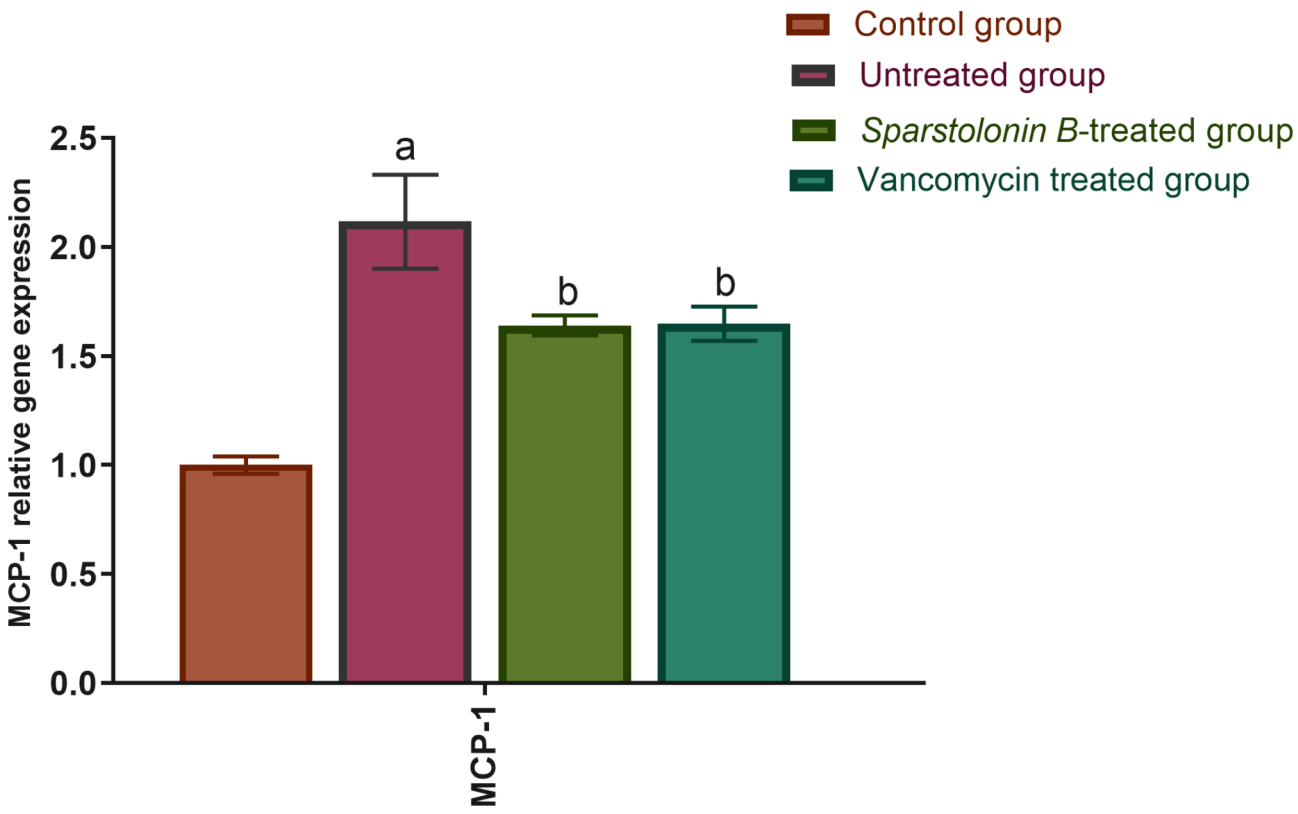

Fig. 6. Relative gene expression MCP-1 in wound tissues of various groups. After making normalization to glyceraldehyde 3-phosphate dehydrogenase (GAPDH), the data indicate a fold difference in expression relative to the natural control group and untreated group. The bars indicate the mean ± SD and are based on the results of four independent investigations. A one-way ANOVA test is employed to measure whether there is a significant change between groups, where: a, $p < 0.05$ when compared to the normal control group on a specified day, b, $p < 0.05$ when compared to the untreated group on a specified day.

Abdul Matin et al. (2022) reported that macrophages play a fundamental role in all stages of the inflammatory responses[28].

Dermal fibroblast cells produce TNF-α, IL-1, and IL-6, which cause neutrophil migration and cause skin damage[29–31]. The histology of the wounds after MRSA-induced superficial skin infection revealed an increase in mast cells and neutrophil infiltration in the upper dermis, which was directly related to the rise in pro-inflammatory cytokines (IL-6, and IL-1). As shown in Fig. 8, groups treated with Vancomycin and sparstolonin B exhibited a significant reduction in pro inflammatory cytokines in contrast to the untreated group ($p > 0.05$) which reveals a wound healing.

Several common bacterial structural patterns, such as peptidoglycan and lipoteichoic acid (LTA) from Gram-positive bacteria, are signalling receptors for TLR-2[4], and participates in the detection of staphylococcal cell wall elements like lipopolysaccharide (LPS)[32,33]. TNF-α was produced by human monocytes in response to LTA generated from *S. aureus*.[4], and animals lacking TLR-2 produced less cytokines in response to *S. aureus* peptidoglycan[33,34]. The adaptor proteins MyD88 and IL-1R-associated kinase (IRAK) allow the TLR family's signalling pathway to activate NF-κB.[33,35,36]. HEK293 and CHO cells have shown that LTA activates NF-B in a TLR-2-dependent manner[4]. This is in line with the findings of our study, which showed that a reduction in TLR-2 was connected to wound healing and the suppression of IL-1 and IL-6 mRNA expression as is presented in (Figs. 5 and 8). Since vancomycin and sparstolonin B both showed anti-inflammatory effects in MRSA skin infections via down-regulating the TLR-2 pathway, sparstolonin B may serve as an alternate antibacterial agent against MRSA for vancomycin-resistant strains.

Furthermore, because MCP-1 is a well-known critical chemokine that regulates monocyte/macrophage migration and infiltration to inflammatory areas due to tissue injury or infection[37]. Additionally, curcumin's effect on fibroblasts suppresses the release of inflammatory mediators by lowering MCP-1 levels, which in turn prevents the infiltration of inflammatory cells both in vitro and in vivo[38]. As depicted in Fig. 6 All treated groups showed significant inhibition of MCP-1 in contrast to the untreated group.

Moreover, the first wave of inflammatory cells is attracted by platelet alpha-granule production of CXCL8, CXCL1, and CXCL2[39–41]. As illustrated in Fig. 7, treatment significantly decreased the relative gene expression of CXCL-1 and CXCL-2 as compared to the untreated group, which in turn decreased the release of inflammatory cells and, consequently, inflammation, which helped the healing process.

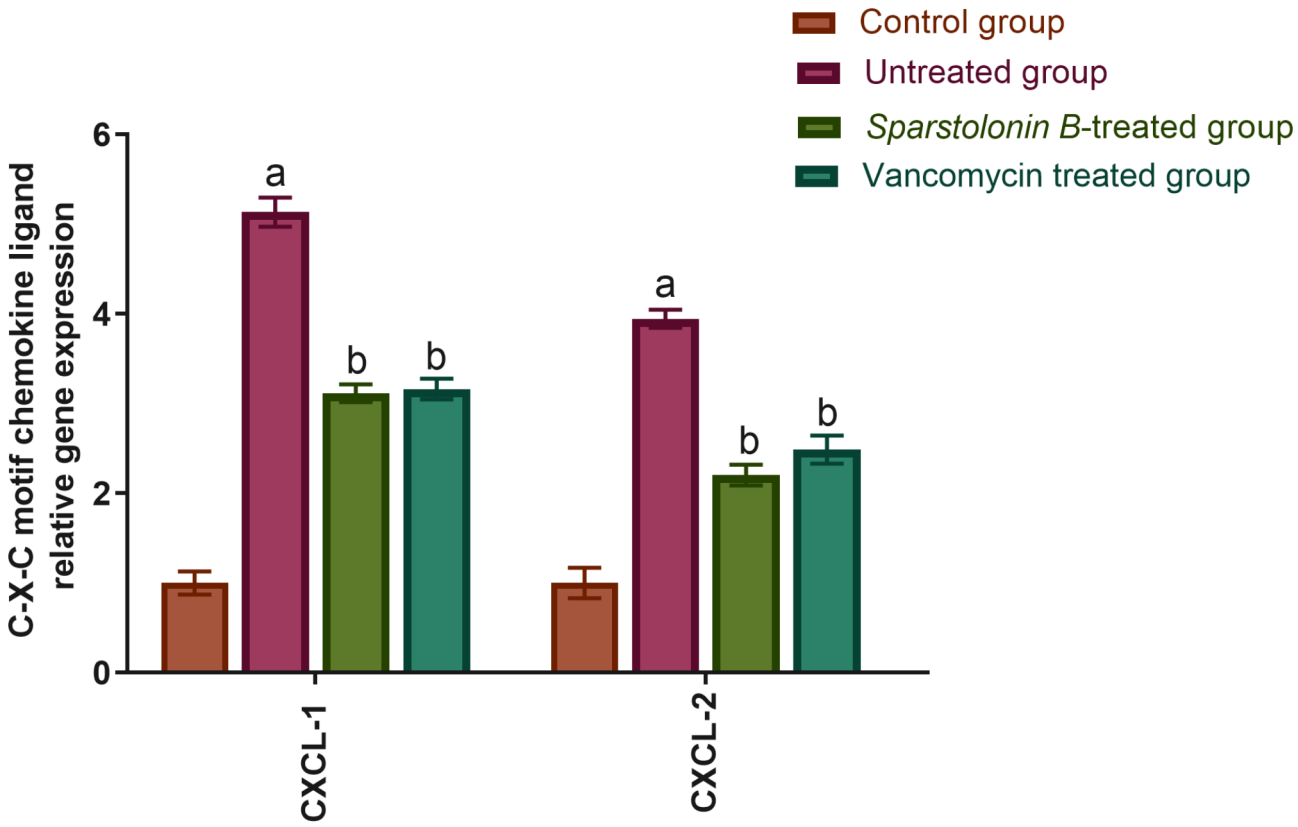

Fig. 7. Relative gene expression C-X-C motif chemokine ligands in wound tissues of various groups. After making normalization to glyceraldehyde 3-phosphate dehydrogenase (GAPDH), the data indicate a fold difference in expression relative to the natural control group and untreated group. The bars indicate the mean ± SD and are based on the results of four independent investigations. A one-way ANOVA test is employed to measure whether there is a significant change between groups, where: a, $p < 0.05$ when compared to the normal control group on a specified day, b, $p < 0.05$ when compared to the untreated group on a specified day.

Computational study

Antibacterial target identification

To tentatively identify the anti-MRSA target of sparstolonine B (SPT-B), we utilized a pharmacophore-based virtual screening approach through the PharmMapper platform [https://www.lilab-ecust.cn/pharmmapper/][16]. PharmMapper predicts likely protein targets for a query molecule by aligning its pharmacophore model's key features, such as the spatial configuration of structural characteristics. Molecules that match these pharmacophore models are more likely to interact with the same protein targets. Thus, the structure of SPT-B was analyzed using PharmMapper to pinpoint potential protein targets related to its antifungal properties. The results were ranked based on their compatibility with the protein target (Fit score; Fig. 11), with a focus on MRSA and *S. aureus* targets. Among the highest-ranking hits, The ATP binding subunit of DNA gyrase (Gyr-B) (PDB ID: 5D7C) was identified, achieving a Fit score of 11.03 (Fig. 11).

Bacterial DNA gyrase, a type II topoisomerase, is essential for DNA replication and transcription. It introduces negative supercoils into DNA using the energy derived from ATP hydrolysis. This enzyme is composed of two subunits: GyrA and GyrB. The GyrB subunit plays a crucial role in ATP binding and hydrolysis, which is necessary for the enzyme's catalytic cycle. Methicillin-resistant Staphylococcus aureus (MRSA) and *S. aureus* have made the study of GyrB particularly important due to the increasing resistance to antibiotics, highlighting the need for new targets for antibacterial therapy[42,43].

GyrB, a 90 kDa protein, is responsible for the ATPase activity of DNA gyrase. It comprises several domains, including the N-terminal ATPase domain and the C-terminal domain involved in DNA binding and interaction with GyrA. The ATPase activity of GyrB is crucial for the energy transduction required for the strand passage mechanism that introduces supercoils into DNA. *S. aureus*, including its methicillin-resistant variant (MRSA), relies on DNA gyrase for survival and proliferation. GyrB, being integral to the function of DNA gyrase, becomes a potential target for antibacterial agents. The essential nature of GyrB in DNA replication and transcription makes it a valuable target, as its inhibition can halt bacterial growth and replication.

MRSA exhibits resistance to many antibiotics, including beta-lactams, due to the mecA gene, which encodes an altered penicillin-binding protein (PBP2a) with low affinity for beta-lactams. However, MRSA still requires DNA gyrase for replication, making GyrB a critical target for new antibiotics. Mutations in GyrB can confer

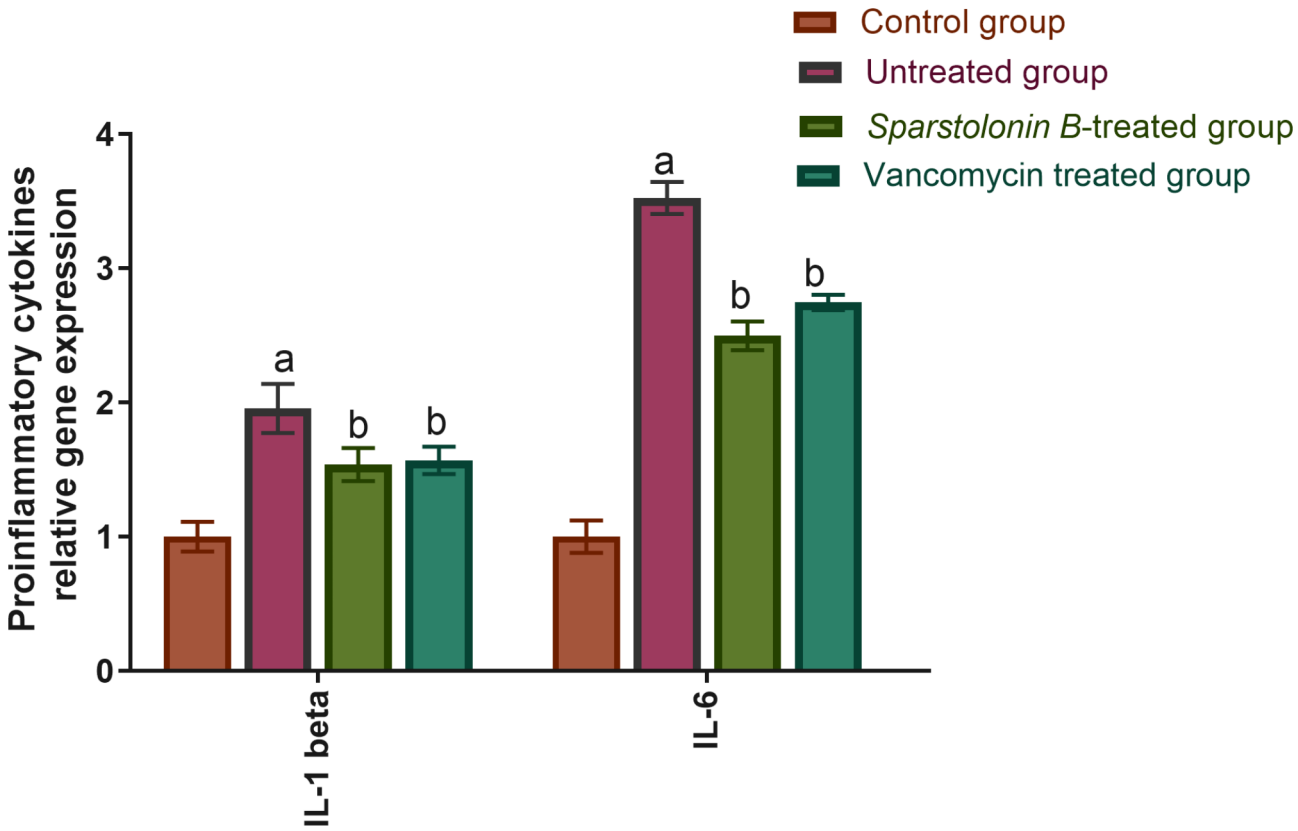

Fig. 8. Relative gene expression proinflammatory cytokines in wound tissues of various groups. After making normalization to glyceraldehyde 3-phosphate dehydrogenase (GAPDH), the data indicate a fold difference in expression relative to the natural control group and untreated group.), the data indicate a fold difference in expression relative to the natural control group and untreated group. The bars indicate the mean ± SD and are based on the results of four independent investigations. A one-way ANOVA test is employed to measure whether there is a significant change between groups, where: a, $p < 0.05$ when compared to the normal control group on a specified day, b, $p < 0.05$ when compared to the untreated group on a specified day.

resistance to fluoroquinolones, a class of antibiotics that target DNA gyrase. These mutations alter the binding site for fluoroquinolones, reducing their efficacy. Therefore, understanding the structure and function of GyrB is essential for developing new drugs that can overcome these resistance mechanisms[42,43].

Several inhibitors targeting GyrB have been developed, including novobiocin and coumermycin, which interfere with ATP binding. These inhibitors have shown efficacy against *S. aureus*, including MRSA strains. However, the emergence of resistance necessitates continuous research and development of novel inhibitors. Recent research focuses on identifying new binding sites and developing inhibitors that can bypass resistance mechanisms. This includes allosteric inhibitors that bind to sites other than the ATPase domain, potentially offering a new avenue for drug development.

The B subunit of bacterial DNA gyrase (GyrB) is a critical enzyme for DNA replication and transcription in *S. aureus* and MRSA. Its essential role and involvement in antibiotic resistance mechanisms make it a promising target for developing new antibacterial agents. Understanding the structure and function of GyrB, as well as the mechanisms of resistance, is vital for designing effective inhibitors that can overcome the challenges posed by antibiotic-resistant bacteria. Continued research and innovation in targeting GyrB hold the potential for significant advancements in treating infections caused by *S. aureus* and MRSA[44].

Docking and molecular dynamics simulation study

To explore the interaction between SPT-B and *S. aureus* Gyr-B (PDB ID: 5D7C), structural models of both were developed and subjected to molecular docking simulations. Ten binding poses were then assessed through short molecular dynamics (MD) simulations lasting 30 ns to determine the most stable binding configuration within the enzyme's active site. The docking pose with the highest score, having an energy value of − 12.67 kcal/mol, demonstrated the greatest stability, as indicated by the lowest root-mean-square deviation (RMSD) throughout the simulation, averaging 1.92 Å (Fig. 12A,B). Consequently, this pose was selected for an extended 200 ns MD simulation to further investigate SPT-B 's binding dynamics within the Gyr-B's active site.

As depicted in Fig. 12C, the RMSD profiles of SPT-B and the co-crystallized inhibitor were notably similar, both averaging an RMSD of approximately 2.27 Å. This consistent binding was reflected in their comparable absolute binding free energies, recorded at − 8.51 and − 8.78 kcal/mol, respectively.

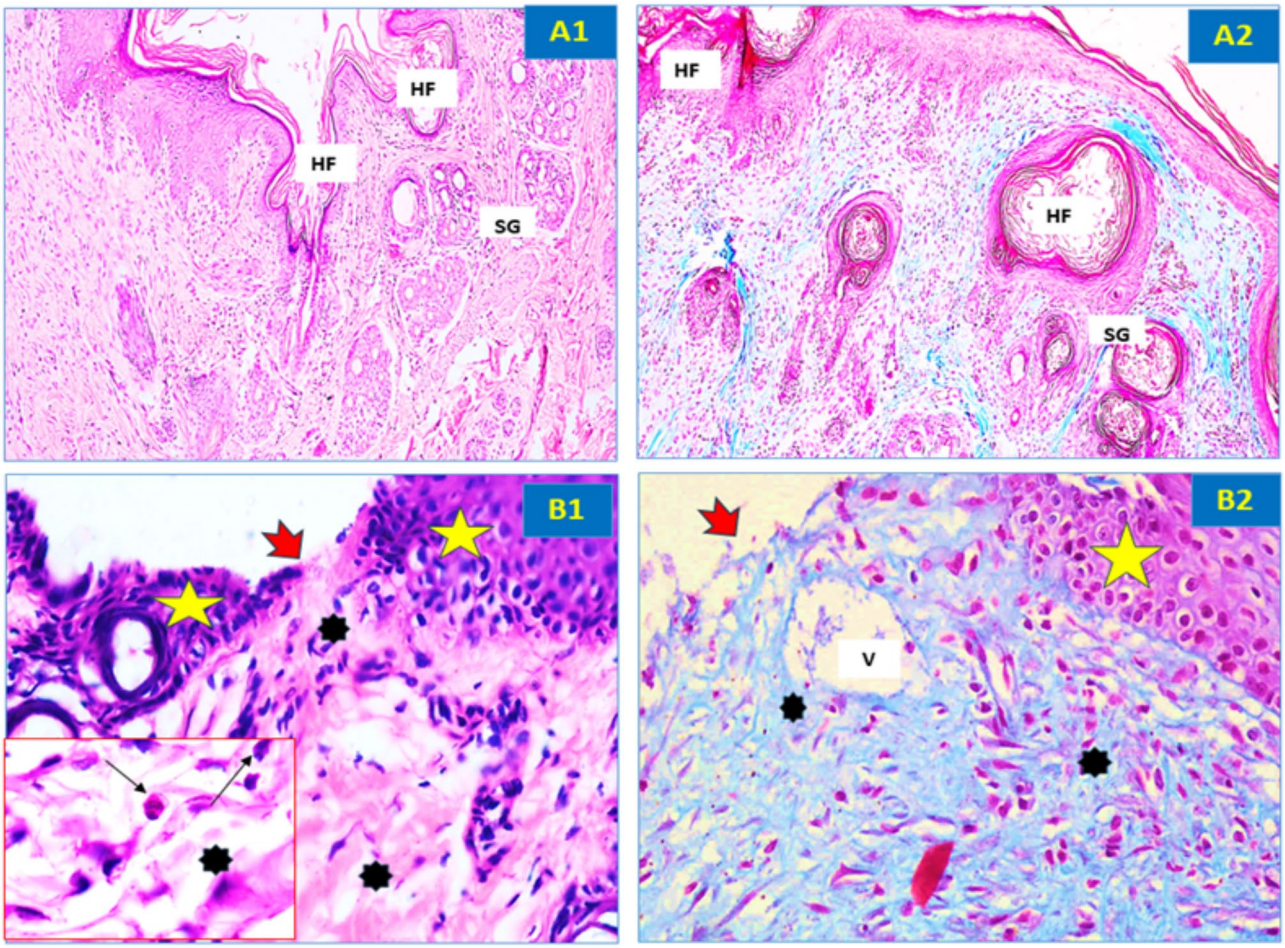

Fig. 9. Photo-micrographic plate 1: A1&A2 control group 1: "A1", stained with H&E; showing the skin covered with normal epidermis formed of stratified squamous keratinized epithelium and dermal connective tissue containing many hair follicles (HF), and sebaceous glands. "A2", stained with Masson trichrome; showing dermal papillae with collagen bundles appear as fine interlacing bundles (PD), and collagen of the reticular dermis appear as coarse wavy bundles (RD), hair follicles (HF) and sebaceous glands (SG). B1&B2 Untreated wound infected group 2; "B1", stained with H&E; showing wound area (notched arrow) and bilateral normal skin (stars). Wound bed is loaded with a dense granulation tissue composed of many connective tissue layers in an acidophilic matrix (asterisks) with inflammatory cellular infiltration mainly neutrophils and eosinophils (linear arrows). "B2" stained with Masson trichrome; showing the dermis composed of collagen bundles compactly organized in abnormal pattern (asterisks). (H&E & Masson trichrome stains × 400).

Further examination of their binding modes revealed that the modeled structure of SPT-B achieved a binding configuration similar to that of the co-crystallized inhibitor. Regarding SPT-B 's binding mode, hydrogen bonding was the predominant interaction within the enzyme's active site. It formed six stable hydrogen bonds with ASN-54, ASP-81, ARG-84, GLY-85, ARG-144, and THR-173. Similar to the co-crystallized inhibitor, SPT-B 's scaffold formed multiple hydrophobic interactions with ILE-86, PRO-87, and ILE-102.

Based on these modeling and MD simulation results, it can be inferred that SPT-B likely exerts its antifungal effects by targeting the MRSA Gyr-B.

Conclusion

The potential wound healing and anti-MRSA activities of sparastolonin was investigated in vivo using an excision wound model and MRSA induction (wound infection model, and peritonitis infection model). In a preliminary assay, sparastolonin B showed a potent antibacterial activity against MRSA. The present findings revealed that sparastolonin B caused tissue repairing and complete wound healing effect after 7 days, with a significant decrease in bacterial count. Furthermore, a computational study was conducted to identify the genes and possible pathways responsible for the anti-MRSA activity of sparastolonin B. Additionally, the most likely molecular targets that could mediate the extract's antibacterial activity were suggested using an inverse docking protocol. Gyr-B was putatively identified to be the most probable target for sparastolonin B. Hence, sparastolonin B can be used as novel anti-dermatophytic agent with potent wound healing, anti-MRSA capacity, which paving the way for future clinical research.

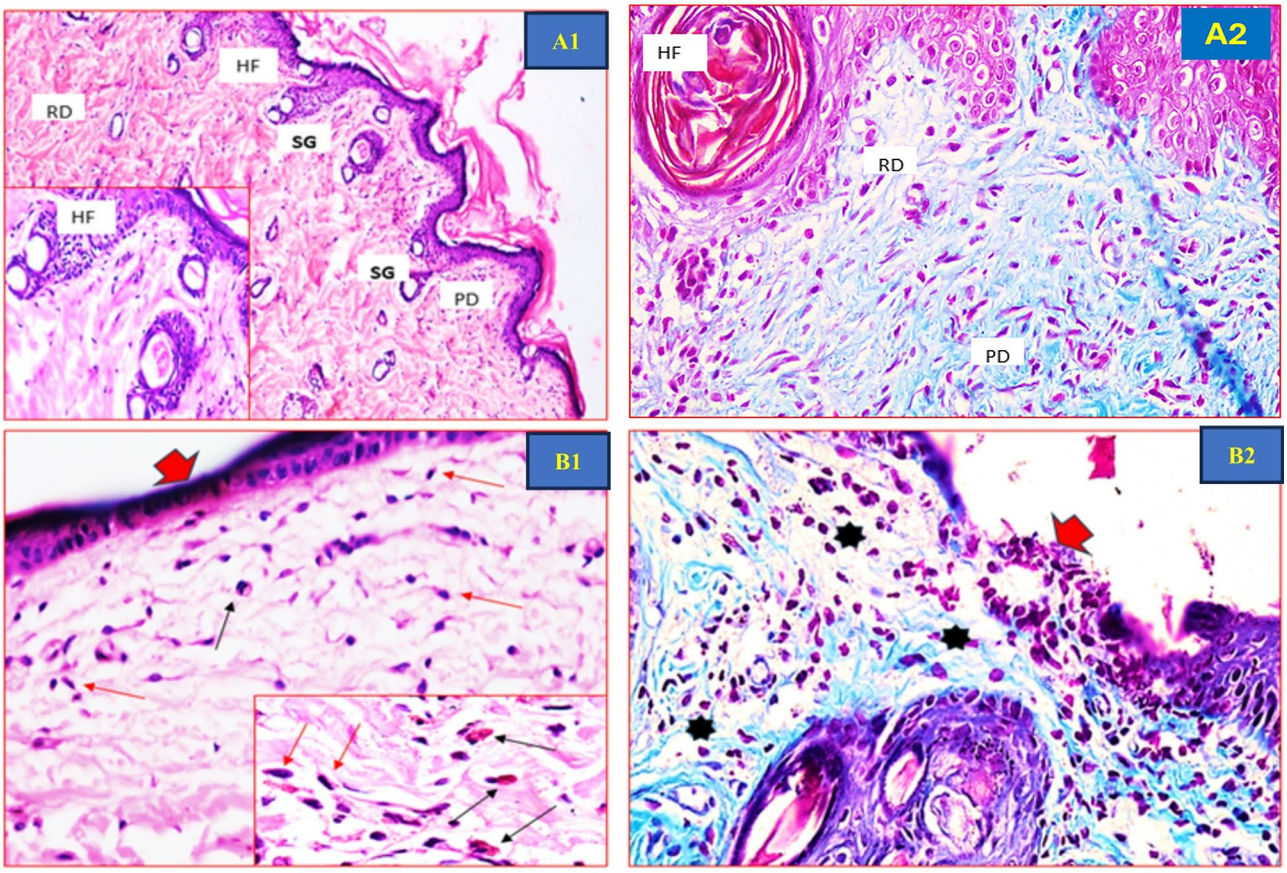

Fig. 10. Photo-micrographic plate II: A1&A2 Sparstolonin B extract-treated group 3; "A1" showing complete re-epithelization of the epidermal defect to be formed of many cell layers. The dermal matrix with many hair follicles (HF) and sebaceous glands (SG). "A2" stained with Masson trichrome; showing collagen bundles in the papillary layer "PD" appear as fine interlacing bundles, and that of the reticular layer "RD" appear as coarse wavy bundles. B1& B2 vancomycin-treated group 4; "B1" stained with H&E; showing incomplete re-epithelization of the wound area "about 1–3 rows" (thick arrow). The dermis showing active elongated, spindle-shaped fibroblasts with basophilic cytoplasm (red linear arrows), neovascularization (BV), Inflammatory cells infiltration mainly macrophages (black linear arrows). B2″; stained with Masson trichrome; showing the dermis with granulation tissue filling the defect having dense collagen arranged in an abnormal pattern (stars). (H&E & Masson trichrome stains × 400).

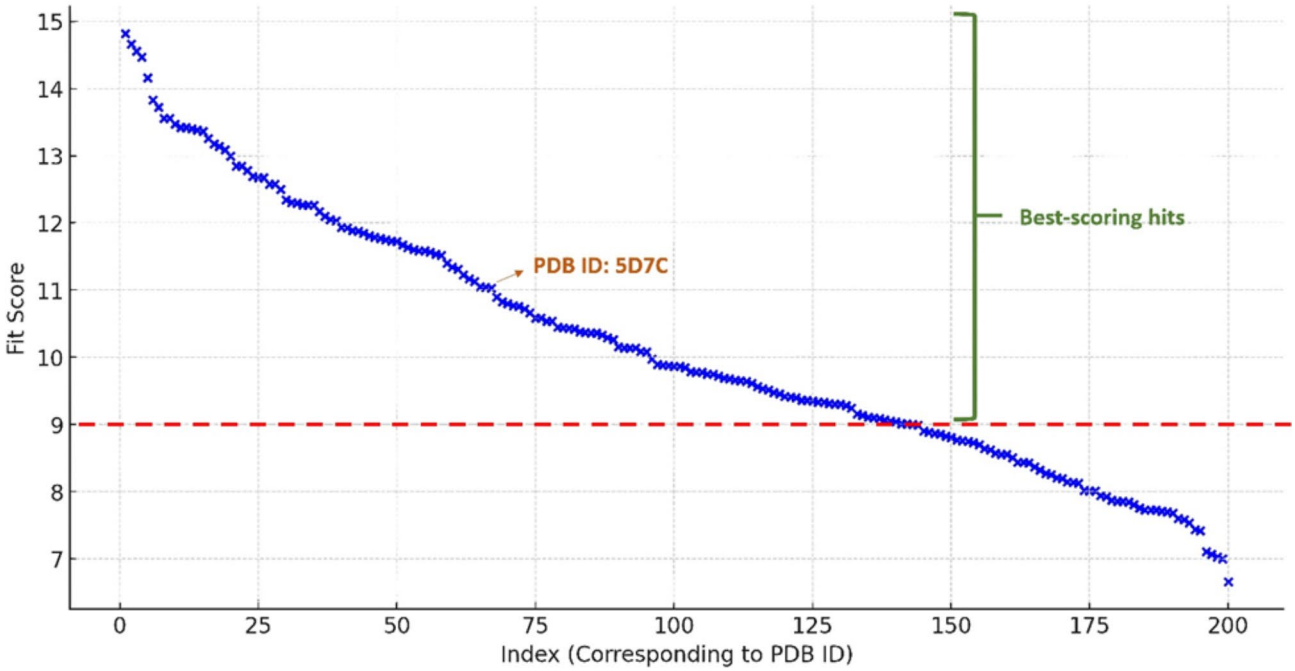

Fig. 11. The PharmMapper results are presented in a scatter plot, showcasing the potential protein targets of SPT-B along with their respective Fit scores. A threshold Fit score of 9 was established as the selection cut-off. Among the top-scoring hits, *S. aureus* Gyr-B (PDB ID: 5D7C) with a Fit score of 11.03, stood out as the sole protein target relevant to the anti-MRSA activity of of SPT-B.

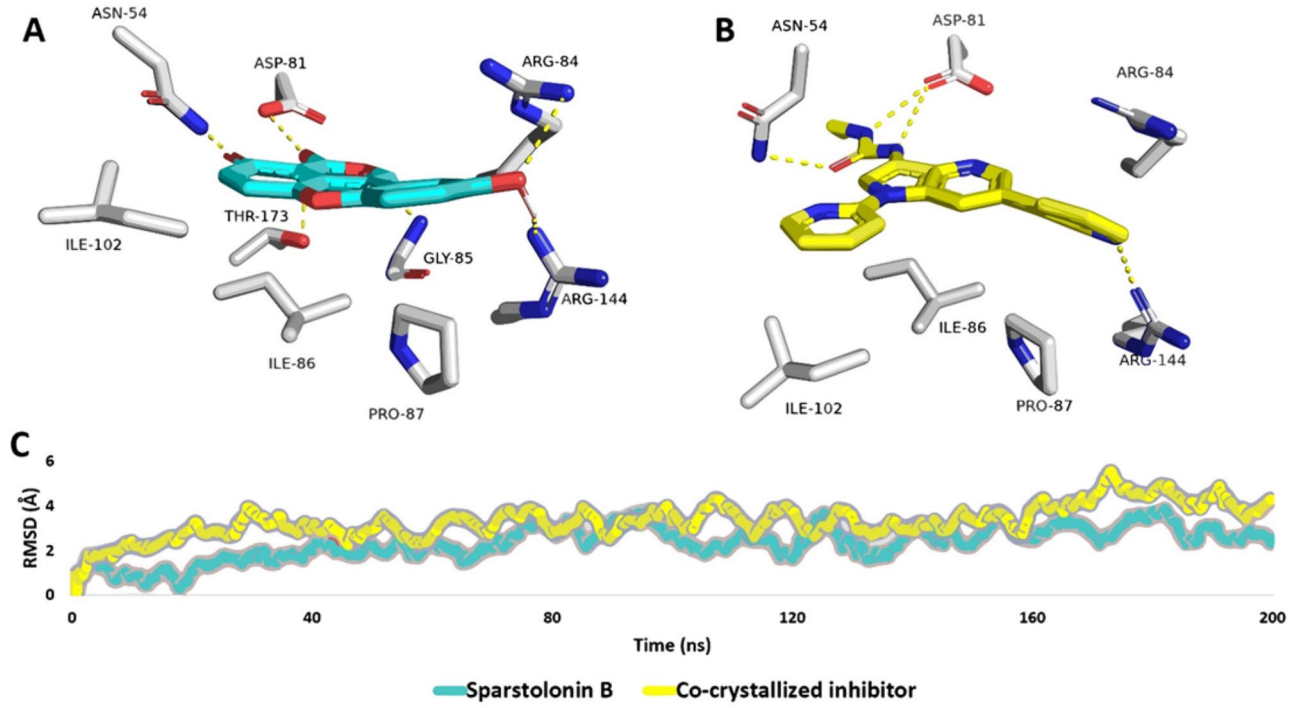

Fig. 12. (**A**,**B**) The most populated poses of SPT-B inside the binding site of *S. aureus* Gyr-B (PDB ID: 5D7C) in comparison with that of the co-crystallized inhibitor. (**C**) RMSDs of SPT-B inside the binding site of *S. aureus* Gyr-B along with that of the co-crystallized inhibitor over the course of 200 ns-long MD simulation.

Data availability

All data generated or analysed during this study are included in this published article.

Received: 14 October 2024; Accepted: 14 February 2025
Published online: 24 September 2025

References

1. Chavakis, T. et al. Staphylococcus aureus extracellular adherence protein serves as anti-inflammatory factor by inhibiting the recruitment of host leukocytes. *Nat. Med.* **8**, 687–693 (2002).
2. Hong, S.-W. et al. Extracellular vesicles derived from Staphylococcus aureus induce atopic dermatitis-like skin inflammation: S. aureus EV in atopic dermatitis. *Allergy* **66**, 351–359 (2011).
3. Miller, L. S. & Cho, J. S. Immunity against Staphylococcus aureus cutaneous infections. *Nat. Rev. Immunol.* **11**, 505–518 (2011).
4. Schröder, N. W. J. et al. Lipoteichoic acid (LTA) of Streptococcus pneumoniaeand Staphylococcus aureus activates immune cells via toll-like receptor (TLR)-2, lipopolysaccharide-binding protein (LBP), and CD14, whereas TLR-4 and MD-2 are not involved. *J. Biol. Chem.* **278**, 15587–15594 (2003).
5. Mullarkey, M. et al. Inhibition of endotoxin response by E5564, a novel toll-like receptor 4-directed endotoxin antagonist. *J. Pharmacol. Exp. Ther.* **304**, 1093–1102 (2003).
6. Tsujimoto, H. et al. Role of toll-like receptors in the development of sepsis. *Shock* **29**, 315–321 (2008).
7. Sun, M.-L. *et al.* Promotion of Wound healing and prevention of frostbite injury in rat skin by exopolysaccharide from the arctic marine bacterium Polaribacter sp. SM1127. *Mar. Drugs* **18**, 48 (2020).
8. Liang, Q. et al. Characterization of Sparstolonin B, a Chinese herb-derived compound, as a selective toll-like receptor antagonist with potent anti-inflammatory properties. *J. Biol. Chem.* **286**, 26470–26479 (2011).
9. Liang, Q. et al. Protective effects of Sparstolonin B, a selective TLR2 and TLR4 antagonist, on mouse endotoxin shock. *Cytokine* **75**, 302–309 (2015).
10. Stenger, M. *et al.* Assessments of thioridazine as a helper compound to dicloxacillin against methicillin-resistant Staphylococcus aureus: In vivo trials in a mouse peritonitis model. *PLoS ONE* **10**, e0135571 (2015).
11. Harikrishnan, L. S. et al. Heterobicyclic inhibitors of transforming growth factor beta receptor I (TGFβRI). *Bioorg. Med. Chem.* **26**, 1026–1034 (2018).
12. Tramontina, V. A. et al. Effect of bismuth subgallate (local hemostatic agent) on wound healing in rats. Histological and histometric findings. *Braz. Dent. J.* **13**, 11–16 (2002).
13. Park, J. Y. et al. Establishment of experimental murine peritonitis model with hog gastric mucin for carbapenem-resistant gram-negative bacteria. *Infect. Chemother.* **49**, 57 (2017).
14. Moore, M. R., Perdreau-Remington, F. & Chambers, H. F. Vancomycin treatment failure associated with heterogeneous vancomycin-intermediate *Staphylococcus aureus* in a patient with endocarditis and in the rabbit model of endocarditis. *Antimicrob. Agents Chemother.* **47**, 1262–1266 (2003).
15. Hummon, A. B., Lim, S. R., Difilippantonio, M. J. & Ried, T. Isolation and solubilization of proteins after TRI zol ® extraction of RNA and DNA from patient material following prolonged storage. *BioTechniques* **42**, 467–472 (2007).
16. Wang, X. et al. PharmMapper 2017 update: A web server for potential drug target identification with a comprehensive target pharmacophore database. *Nucleic Acids Res.* **45**, W356–W360 (2017).
17. Eberhardt, J., Santos-Martins, D., Tillack, A. F. & Forli, S. AutoDock Vina 1.2.0: New docking methods, expanded force field, and python bindings. *J. Chem. Inf. Model.* **61**, 3891–3898 (2021).
18. Seeliger, D. & De Groot, B. L. Ligand docking and binding site analysis with PyMOL and Autodock/Vina. *J. Comput. Aided Mol. Des.* **24**, 417–422 (2010).
19. Phillips, J. C. et al. Scalable molecular dynamics with NAMD. *J. Comput. Chem.* **26**, 1781–1802 (2005).
20. Ribeiro, J. V. et al. QwikMD—integrative molecular dynamics toolkit for novices and experts. *Sci. Rep.* **6**, 26536 (2016).
21. Humphrey, W., Dalke, A. & Schulten, K. VMD: Visual molecular dynamics. *J. Mol. Graph.* **14**, 33–38 (1996).
22. Miller, B. R. et al. *MMPBSA.py*: An efficient program for end-state free energy calculations. *J. Chem. Theory Comput.* **8**, 3314–3321 (2012).
23. Li, J., Chen, J. & Kirsner, R. Pathophysiology of acute wound healing. *Clin. Dermatol.* **25**, 9–18 (2007).
24. Tsuboi, R. & Rifkin, D. B. Recombinant basic fibroblast growth factor stimulates wound healing in healing-impaired db/db mice. *J. Exp. Med.* **172**, 245–251 (1990).
25. Raczyńska-Witońska, G. & Witoński, D. Fungi and bacteria as a pathogenic factor in wound healing in patients after orthopaedic surgeries. *Ortop. Traumatol. Rehabil.* **8**, 646–649 (2006).
26. Phillips, D. & Davey, C. Wound cleaning versus wound disinfection: A challenging dilemma. *Perspectives* **21**, 15–16 (1997).
27. Kim, N., Kim, C., Ryu, S. H., Kim, G. O. & Bae, J.-S. Anti-inflammatory effect of sparstolonin B through inhibiting expression of NF-κB and STAT-1. *IJMS* **23**, 10213 (2022).
28. Matin, M. A., Hossen, M. J., Ahmed, Md. S., Rahman, M. & Sikder, M. H. The role of macrophages in inflammation. in *Recent Advancements in Microbial Diversity* 53–71 (Elsevier, 2022). https://doi.org/10.1016/B978-0-12-822368-0.00004-9.
29. Mason, M. J. & Van Epps, D. E. In vivo neutrophil emigration in response to interleukin-1 and tumor necrosis factor-alpha. *J. Leukoc. Biol.* **45**, 62–68 (1989).
30. Fahey, T. J. et al. Cytokine production in a model of wound healing: The appearance of MIP-1, MIP-2, cachectin/TNF and IL-I. *Cytokine* **2**, 92–99 (1990).
31. Robertson, F. M. et al. Interleukin-1α gene expression during wound healing. *Wound Rep. Regen.* **3**, 473–484 (1995).
32. Lien, E. et al. Toll-like receptor 2 functions as a pattern recognition receptor for diverse bacterial products. *J. Biol. Chem.* **274**, 33419–33425 (1999).
33. Takeuchi, O. et al. Differential roles of TLR2 and TLR4 in recognition of gram-negative and gram-positive bacterial cell wall components. *Immunity* **11**, 443–451 (1999).
34. Takeuchi, O. et al. Cutting edge: Preferentially the *R*-stereoisomer of the mycoplasmal lipopeptide macrophage-activating lipopeptide-2 activates immune cells through a toll-like receptor 2- and MyD88-dependent signaling pathway. *J. Immunol.* **164**, 554–557 (2000).
35. Medzhitov, R. et al. MyD88 Is an adaptor protein in the hToll/IL-1 receptor family signaling pathways. *Mol. Cell* **2**, 253–258 (1998).
36. Muzio, M., Natoli, G., Saccani, S., Levrero, M. & Mantovani, A. The human toll signaling pathway: Divergence of nuclear factor κB and JNK/SAPK activation upstream of tumor necrosis factor receptor–associated factor 6 (TRAF6). *J. Exp. Med.* **187**, 2097–2101 (1998).
37. Deshmane, S. L., Kremlev, S., Amini, S. & Sawaya, B. E. Monocyte chemoattractant protein-1 (MCP-1): An overview. *J. Interferon Cytokine Res.* **29**, 313–326 (2009).
38. Dai, X. et al. Nano-formulated curcumin accelerates acute wound healing through Dkk-1-mediated fibroblast mobilization and MCP-1-mediated anti-inflammation. *NPG Asia Mater.* **9**, e368–e368 (2017).
39. Gleissner, C. A., Von Hundelshausen, P. & Ley, K. Platelet chemokines in vascular disease. *ATVB* **28**, 1920–1927 (2008).
40. Kobayashi, Y. The role of chemokines in neutrophil biology. *Front Biosci* **13**, 2400 (2008).

41. Wetzler, C., Kämpfer, H., Stallmeyer, B., Pfeilschifter, J. & Frank, S. Large and sustained induction of chemokines during impaired wound healing in the genetically diabetic mouse: Prolonged persistence of neutrophils and macrophages during the late phase of repair. *J. Investig. Dermatol.* **115**, 245–253 (2000).
42. Zhang, J. et al. Discovery of azaindole ureas as a novel class of bacterial gyrase B inhibitors. *J. Med. Chem.* **58**, 8503–8512 (2015).
43. Barančoková, M., Kikelj, D. & Ilaš, J. Recent progress in the discovery and development of DNA gyrase B inhibitors. *Future Med. Chem.* **10**, 1207–1227 (2018).
44. Azam, M. A., Thathan, J. & Jubie, S. Dual targeting DNA gyrase B (GyrB) and topoisomerse IV (ParE) inhibitors: A review. *Bioorg. Chem.* **62**, 41–63 (2015).

Acknowledgements
We thank Deraya University for laboratory space. The used MRSA strain was kindly provided by from Minia University Hospital (isolated from pus)."

Author contributions
Conceptualization: URA, AHE, KA; methodology: AHE,KA, ASM, MA, RY, FAM; software: AHE, FA, MYB, SYA, FHA; formal analysis: AHE, MAA, EAS, MAE, AMS; investigation: URA, KA; resources: AHE, ASM, MA; data curation: AHE, MAA, EAS, MAE, AMS; writing—original draft: AHE, KA, ASM, MA, RY, FAM.; writing—review and editing: URA, KA, AHE. All authors have read and agreed to the published version of the manuscript.

Declarations

Competing interests
The authors declare no competing interests.

Additional information
Correspondence and requests for materials should be addressed to U.R.A.

Reprints and permissions information is available at www.nature.com/reprints.

Publisher's note Springer Nature remains neutral with regard to jurisdictional claims in published maps and institutional affiliations.